Meteoritics & Planetary Science 51, Nr 6, 1184–1200 (2016)
doi: 10.1111/maps.12651

Report

Petrology and oxygen isotopic compositions of clasts in HED polymict breccia NWA 5232

Katrina D. VAN DRONGELEN[1,*], Douglas RUMBLE III[2], and Kimberly T. TAIT[3]

[1]Department of Earth Sciences, University of Toronto, Toronto, Ontario M5S 3B1, Canada
[2]Geophysical Laboratory, Carnegie Institution of Washington, Washington, District of Columbia 20015, USA
[3]Royal Ontario Museum, Department of Natural History, Toronto, Ontario M5S 2C6, Canada
[*]Corresponding author. E-mail: k.vandrongelen@es.utoronto.ca

(Received 14 April 2014; revision accepted 01 March 2016)

Abstract–Northwest Africa (NWA) 5232, an 18.5 kg polymict eucrite, comprises eucritic and exogenic CM carbonaceous chondrite clasts within a clastic matrix. Basaltic clasts are the most abundant eucritic clast type and show a range of textures and grain size, from subophitic to granoblastic. Other eucritic clast types present include cumulate (high-En pyroxene), pyroxene-lath, olivine rich with symplectite intergrowths as a break-down product of a quickly cooled Fe-rich metastable pyroxferroite, and breccia (fragments of a previously consolidated breccia) clasts. A variable cooling rate and degree of thermal metamorphism, followed by a complex brecciation history, can be inferred for the clasts based on clast rounding, crystallization (and recrystallization) textures, pyroxene major and minor element compositions, and pyroxene exsolution. The range in $\delta^{18}O$ of clasts and matrix of NWA 5232 reflects its origin as a breccia of mixed clasts dominated by eucritic lithologies. The oxygen isotopic compositions of the carbonaceous chondrite clasts identify them as belonging to CM group and indicate that these clasts experienced a low degree of aqueous alteration while part of their parent body. The complex evolutionary history of NWA 5232 implies that large-scale impact excavation and mixing was an active process on the surface of the HED parent body, likely 4 Vesta.

INTRODUCTION

The howardite–eucrite–diogenite (HED) clan of meteorites comprises the eucrites, diogenites, and polymict breccias and represents the most extensive collection of samples from any differentiated extraterrestrial body (Warren et al. 2009). They are linked by a common mass-dependant oxygen isotope fractionation line (Wiechert et al. 2004; Greenwood et al. 2005), suggesting a common origin from a large differentiated body, possibly the asteroid 4 Vesta (e.g., Binzel and Xu 1993). The eucrites consist of basaltic and gabbroic lithologies, likely from basaltic flows and shallow to deep intrusions on the eucrite parent body (EPB) (Duke and Silver 1967). The diogenites consist of ultramafic rocks (orthopyroxenites, olivine-bearing orthopyroxenites, harzburgites, and dunites) and are interpreted to have formed deep in the crust of the EPB (Mittlefehldt et al. 1998; Shearer et al. 2010; Beck et al. 2011). The eucrites can be subdivided into two groups: cumulate and basaltic, typically distinguished by their pyroxene major element contents, bulk trace and major elements, and textures (Takeda 1997; Mittlefehldt et al. 1998). In most cases, these lithologies have been affected by thermal metamorphism, brecciation, and shock while part of the EPB (Takeda and Graham 1991).

The HED polymict breccias are fragmental and regolith breccias generated by impact and primarily comprise fragments of eucritic and diogenitic material embedded in a fine-grained matrix (Mittlefehldt et al. 2013). These breccias constitute a spectrum from

polymict eucrites, through howardites, to polymict diogenites. Polymict eucrites are typically described as HED polymict breccias that contain <10 vol% diogenitic material, howardites contain >10 vol% diogenitic material, and polymict diogenites contain <10% eucritic material (Delaney and Prinz 1984). In addition to HED lithologies, HED polymict breccias may also contain impact melt clasts and exogenic material (e.g., carbonaceous chondrite) (Zolensky et al. 1996).

Northwest Africa (NWA) 5232 is an 18.5 kg polymict eucrite (Fig. 1), containing a variety of basaltic and cumulate eucritic clasts and no diogenitic material. This large HED meteorite is a regolith breccia (Cartwright et al. 2013), generated by impact mixing at or near the surface of the EPB (Bischoff and Stöffler 1992), as it includes significant exogenic material (carbonaceous chondrite fragments derived from an impactor). The purpose of this study is to establish the diversity of clasts present in this large breccia by review of clast textures, mineral compositions, and oxygen isotopic analyses of individual clasts. This study will add to the understanding of the composition and constituents of the EPB surface regolith, as well as the degree of impact processing and mixing that the surface of this asteroid experienced. Polymict breccias likely constitute much of the surface of 4 Vesta, so defining the heterogeneity of regolithic breccias, such as NWA 5232, has particular relevance for the interpretation of remote sensing data acquired by the Dawn spacecraft, which primarily observed the surface of 4 Vesta (De Sanctis et al. 2012; Mittlefehldt et al. 2013).

SAMPLE AND ANALYTICAL METHODS

The entire main mass of NWA 5232, including all cuts made from this mass, was available for this study. Two large slices of NWA 5232 were cut with a low-loss diamond wire saw from the main mass, and six polished thin sections were prepared from part of this material. The polished sections were examined with a petrographic microscope, electron microprobe (EMP), scanning electron microscope (SEM), and Raman spectrometer.

For pyroxene and plagioclase mineral compositions, a Cameca SX50 EMP was used with a 1 μm beam, accelerating potential of 15 keV, and beam current of 15 nA. Counting times were 20 s, and all reported analyses have good oxide totals (>98%) and stoichiometry. Natural and synthetic phases of well-known compositions were used as standards, and data were corrected using a ZAF program. All pyroxene analyses were corrected for Fe^{3+} and projection onto the pyroxene quadrilateral using the method described by Lindsley (1983). Compositional ternary (and quadrilateral) plots were created using Tri-plot (Graham and Midgley 2000). To examine clast textures and identify accessory phases, backscattered electron (BSE) images were collected and energy dispersive spectrometer (EDS) semiquantitative analyses were performed with a JEOL JSM-6610LV SEM. A Horiba LabRAM Aramis confocal Raman spectrometer with mapping stage was used to identify mineral precipitates, resulting from terrestrial weathering using the 532 nm laser, 200 μm hole, 150 μm slit, 50× magnification, and no filter (100% laser power). Modal abundances of clasts were estimated for BSE images using ImageJ (free image processing software), similar to the method described by Liu et al. (2009). For each BSE image reviewed, grayscale ranges for the mineral phases were established using the identifications made by semiquantitative EDS. The relative abundance of each mineral phase was measured as the number of pixels within the specified grayscale range divided by the number of pixels for the image as a whole (blank space and holes subtracted). Images used for these measurements were at low magnification (<200×) to maximize the degree of representativeness and consisted entirely of the clast (no matrix). These modal abundances should be considered as estimates as grayscale ranges were set visually and do not take into account phases that may overlap with respect to grayscale (e.g., terrestrial calcite and melt veins). Clast sizes given are minimum estimates as they are measured in thin section and on cut faces of the sample. The classification and distribution of clasts must be interpreted with caution due to the small clast sizes, heterogeneous distribution of clasts, and variability in grain size that may reasonably exist on a relatively small scale within an igneous system. Apparent exsolution lamellae widths, measured in BSE images, are maximums as they are measured from randomly oriented pyroxenes in thin section.

Oxygen isotope ratios were measured at the Geophysical Laboratory, Carnegie Institution of Washington. Three preliminary samples were analyzed (labeled "Bulk" in Table 3) in preparation for further work and consisted of one carbonaceous chondrite and two eucritic samples. The bulk samples were received as 1 mm grains, crushed under ethanol in a boron nitride mortar and pestle, and ultrasonicated in dilute HCl. The bulk carbonaceous chondrite grains were hand-picked by A. J. Irving, avoiding eucritic components. The bulk eucritic samples included both breccia matrix and eucritic clasts. The set of samples designated with a letter (e.g., NWA 5232_a) were obtained using a diamond-tipped drill to extract powered samples from 1 mm diameter holes of individual clasts from a single

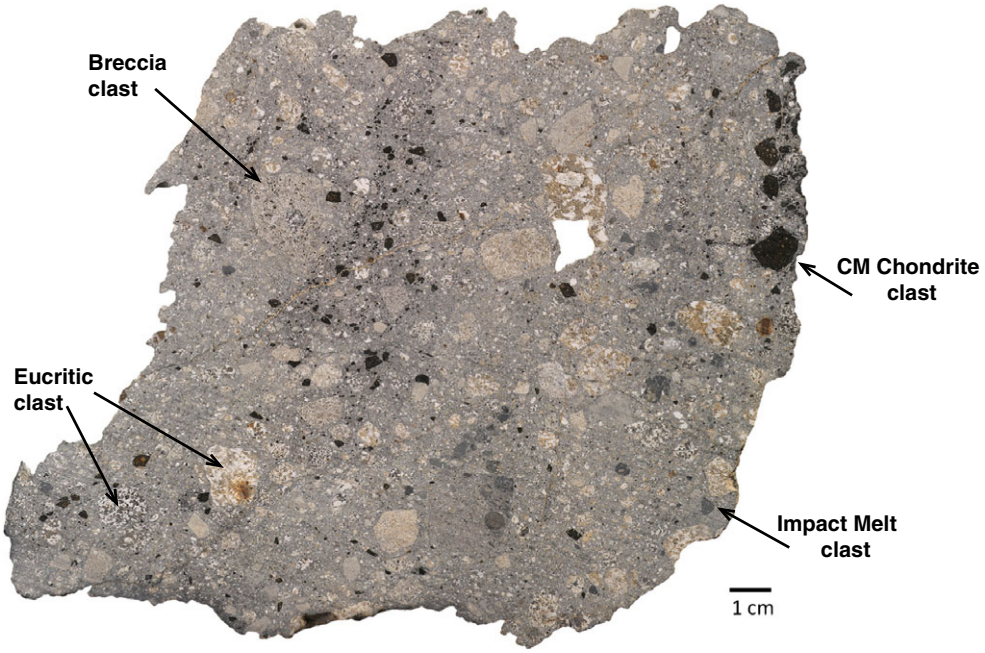

Fig. 1. Photograph of a large slice of NWA 5232 showing brecciated nature of the sample. Clasts with intergrowths of white and black or white and brown minerals are eucritic. Other clast types include dark gray impact melt clasts, black carbonaceous chondrite clasts, and breccia clasts. Note the heterogeneous distribution of components, such as carbonaceous chondrite fragments. Large white areas in top-right quadrant are holes in the slice.

slice of NWA 5232 (sample locations are shown in supporting information). The slice was taken from the end of the stone (near the weathered surface). The weathered side of the slice is irregular, is smoothly rounded, and shows little fusion crust. The cut side is cross-cut by one vein of terrestrial calcite 0.5 mm in thickness, which was avoided when drilling samples. A second set of samples (those with a number designation) were obtained from interior slices of NWA 5232 as 24–80 mg chips of individual clasts, removed by diamond-tipped drill. These samples were crushed in an alumina mortar and pestle, and subsamples of this material were used for oxygen isotope analyses. Powder samples of 2.5–4.0 mg were compacted into sample holders with a stainless steel rod and dried in an oven for 2 days. Dried holders with 12 individual samples were loaded for isotopic analysis in a reaction chamber designed by Sharp (1990). The reaction chamber with samples loaded was heated and evacuated for several hours, repeatedly fluorinated with 25 torr of BrF_5, and evacuated, and then fluorinated overnight. Evacuation and fluorination were repeated the next morning until measured room-temperature fluorination products, noncondensable in liquid nitrogen, were reduced to a negligible blank.

Analysis of individual samples was made by loading 25–30 torr of BrF_5 into the reaction chamber and heating the sample with an infrared laser (Synrad Inc.; 30 watt, CO_2 laser, 10.6 μm wavelength). The spot size of the laser beam was defocused to a 100 μm diameter to minimize scattering of sample particles. The resulting mixture of O_2, SiF_4, and residual interhalogen compounds was purified by passage through two liquid nitrogen traps and pumped by a single-stage mercury diffusion pump onto molecular sieve 5A chilled by liquid nitrogen. The purified sample was transferred to the dual inlet of a Thermo-Fisher MAT 252 mass spectrometer, where the ion beams of $^{16}O^{16}O$, $^{16}O^{17}O$, and $^{16}O^{18}O$ were measured (Rumble and Hoering 1994). Every sample was tested for NF_3 and CF_4 contamination by scanning the mass range from 40 to 75 daltons with a Faraday cup whose preamplifier resistor had a value of 3×10^{11} ohms.

Two aliquots of a reference material, Gore Mountain garnet (USNM 107144, obtained by courtesy of J. Post, Smithsonian Institution), were analyzed for every four unknowns. The reference garnet gives a value of $\delta^{18}O_{VSMOW}$ of 6.0‰ in comparison to UWG-2 (Rumble et al. 1997; Valley et al. 1995). The two sigma standard deviations of Gore Mountain garnet analyses measured during the course of this study were as follows: $\Delta^{17}O \pm 0.03$, $\delta^{17}O \pm 0.09$, and $\delta^{18}O \pm 0.17$‰. The value used for the slope of the terrestrial fractionation line (TFL) in this study is 0.526 (±0.001) (Rumble et al. 2007). Limitations on sample size from drill holes and from whole clast samples prevented

replicate analyses except for NWA 5232-10 (pyroxene lath), where duplicate analyses gave the following results: $\delta^{17}O = 1.62 \pm 0.04$, $\delta^{18}O = 3.38 \pm 0.02$, and $\Delta^{17}O = -0.16 \pm 0.03‰$.

RESULTS AND DISCUSSION

Overview of Sample

NWA 5232 (Fig. 1) comprises eucritic, carbonaceous chondrite, and impact melt clasts and mineral fragments set in a fine- to medium-grained clastic matrix (e.g., Metzler et al. 1995). The sample is poorly sorted in its size distribution of material. For this study, to assist with the descriptions of the different components of the meteorite, clasts will be defined as coherent material if >500 μm in size, whereas fragments <500 μm in size are regarded as part of the matrix. The eucritic clasts show a variety of basaltic and gabbroic textures and range in size from 500 μm to 4.2 cm (average 0.5 cm). The lithic clasts also include breccia clasts, which are clasts of a previous HED breccia that became consolidated and subsequently incorporated as a clast.

The matrix of NWA 5232 is fine to medium grained, containing fragments of single crystals and lithic material, and grades from fine grains to clasts in size. In addition to clasts of carbonaceous chondrite material, small (<500 μm) fragments of carbonaceous chondrites are mixed irregularly into the matrix material. The matrix is light gray in overall appearance, consists primarily of plagioclase and pyroxene, and is homogeneous in appearance with the exception of pockets enriched in carbonaceous chondrite fragments, which are darker in color and appear to be a later fill (Fig. 1).

The interior texture of the sample is visible over much of the surface of the main mass due to the loss of the fusion crust. On one side of the main mass, a large rust-stained area (5.5 × 6 cm) can be observed that contains a large high relief concentration of metal. This rust-stained area is surrounded by a dark glassy rim and is a discrete clast with abundant metal, clasts, and veins cross-cut by the dark glassy rim. Similar small rust-stained clasts were observed in cut material and were identified as carbonaceous chondrite material or metal-rich eucritic clasts.

NWA 5232 experienced terrestrial weathering in a hot desert environment. Approximately 70% of the fusion crust has been lost, and wind ablated grooves have developed on the majority of the surface lacking fusion crust. Factures are filled with terrestrial calcite, as is frequently observed as a consequence of weathering in hot deserts (Crozaz et al. 2003). The fractures are pervasive and calcite is present as large inter-grain and fine intra-grain veins. Minor oxidation of metal in carbonaceous chondrite and metal-rich eucritic clasts is evidenced by an iron staining surrounding this material. Overall, the degree of weathering is comparable to W2, using the Wlotzka (1993) weathering scale for ordinary chondrites.

Eucritic Clast Textures

The primary aim of this study was to establish the degree of variation present in a large HED polymict breccia by examination of textures and mineral compositions of clasts. The eucritic clasts of NWA 5232 can be broadly grouped into six types based on their textures and mineral constituents: (1) subophitic, (2) granoblastic, (3) cumulate, (4) pyroxene lath, (5) olivine rich, and (6) breccia clasts. Of the 42 clasts examined in detail, 23 belonged to the subophitic group (12 coarse-, 5 medium-, and 6 fine-grained), 7 to the granoblastic group (4 coarse-, 2 medium-, and 1 fine-grained), 2 to the breccia clast group, 1 to the cumulate eucrite clast group, 1 to the olivine-rich group, 1 to the pyroxene-lath group, 1 was an impact melt clast, and 6 were single-crystal clasts (4 of which compositionally fit with the coarse-grained subophitic groups). These eucritic clast textural types can be further subdivided into 20 distinct groups within these broad types, based on their textures and compositions; this article will focus on the six broad types. No diogenitic material was identified.

Subophitic Clasts

Of the 42 clasts examined in detail in polymict eucrite NWA 5232, 23 have a subophitic texture, making this the most abundant textural type in this breccia. The subophitic clasts are the most variable in crystal coarseness (Table 1), from narrow acicular (Fig. 2A) to large tabular plagioclase (Fig. 2B), suggesting variable cooling rates from a melt (relatively rapid to slow, respectively). The acicular subophitic clasts contain pyroxene, silica, and opaques interstitial to long (up to 0.5 mm), randomly oriented, needle-like plagioclase. The interstitial pyroxenes exhibit thin exsolution lamellae and evidence of remnant igneous zoning in the varying concentration of lamellae from grain contact with plagioclase outwards (higher Ca content at contact, exsolving more abundant high-Ca pyroxene lamellae), similar to remnant zoning reported in Yamaguchi et al. (2009). The presence of this remnant zoning suggests that this lithology experienced relatively lower degrees of thermal metamorphism as compared with the other clasts discussed in this article (Yamaguchi et al. 2009).

Table 1. Petrographic description summary.

Clast type	Clast subtype	Clast shape	Clast size (mm)	Modal abundances (vol%)/sizes (μm)					Accessory types	Figure
				Plagioclase	Pyroxene	Silica	Olivine	Accessory		
Subophitic				30–55%	30–65%	3–15%	0%	Tr-2%		
	Acicular	Subangular	0.5–6.5	10–500	50–300	5–100		5–100	Chr, Il	2A
	Medium	Subangular	3.0–7.5	75–300	<400	<100		10–100	Tr, Chr, Il	Supp.
	Coarse	Rounded-subrounded	0.5–20.0	150–1200	<500	<100		1–100	Tr, Il, Chr, Bad	2B
Granoblastic				40–50%	40–50%	7–15%	0%	Tr-1%		
	Fine	Angular-subangular	1.0–12.0	30–300	50–100	5–70		5–50	Il, Tr, Chr, Zr	3A
	Coarse	Rounded	5.5–8.5	<1500	<750	<400		30–350	Il, Tr, Chr	3B
Cumulate clast				54%	40%	6%	0%	Tr		
		Subrounded	6.0–7.0	100–1200	300–800			5–50	Chr, Il, Tr	4
Pyroxene-lath				37%	61%	0%	0%	2%		
		Angular	2.0–6.5	30–200	10–100	–		2–20	Il, Fe-Ni, Chr	5
Olivine rich				0%	70%	10%	15%	5%		
		Rounded	1.5–2.0		50–100	10–100	10–100		Il	6

Petrographic descriptions are for clast group examples within each subtype. Accessory minerals include chromite (Chr), ilmenite (Il), troilite (Tr), Fe-Ni metal (Fe-Ni), baddeleyite (Bad), and zircon (Zr). Clast sizes for subtypes are ranges within groups or, for those types of a single individual, smallest and largest dimension. Figure presented in supporting information is listed as "Supp."

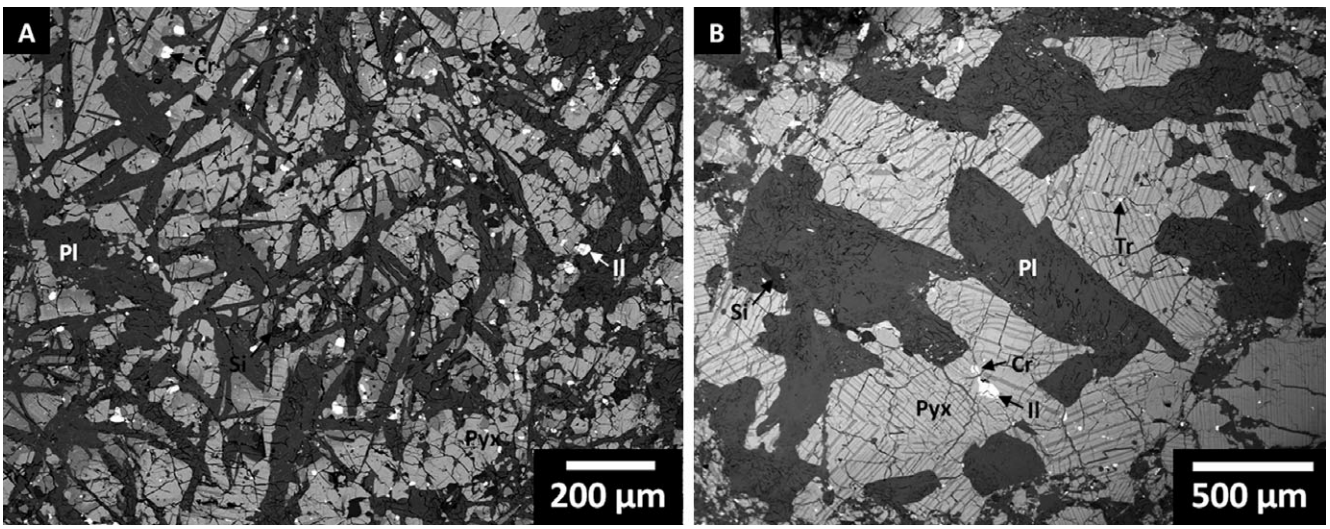

Fig. 2. Backscattered electron (BSE) images of two subophitic clasts. The silicates in these clasts are pyroxene (Pyx) (with darker high-Ca exsolution lamellae), plagioclase (Pl), and silica (Si). White phases are opaques: chromite (Cr) ± ilmenite (Il) ± troilite (Tr). A) Acicular-plagioclase subophitic clast. B) Coarse-grained subophitic clast.

The coarse subophitic clasts contain plagioclase that are large and tabular and contain numerous fine (<20 μm) pyroxene inclusions (Fig. 2B). These anhedral pyroxene inclusions are often elongated or concentrated into strings and are either present throughout the plagioclase grains or restricted to grain edges. The pyroxene exsolution lamellae thicknesses vary between clast groups and are often displaced along intracrystalline fractures or bent, likely by shock. The medium-grained subophitic clasts are intermediate in coarseness between the acicular and coarse-grained subophitic clasts, but are most similar to the coarse subophitic clasts (see supporting information). Some medium subophitic clasts exhibit granoblastic concentrations of silica, high-Ca pyroxene, and opaque minerals, which may be the product of late-stage crystallization. Some of the medium- and coarse-grained subophitic clasts show an additional set of very fine (<1 μm) high-Ca pyroxene exsolution lamellae at an angle to the larger lamellae. This second set of fine

lamellae are the result of continued exsolution of high-Ca pyroxene after the original pigeonite inverted to hypersthene, along a different (orthopyroxene) crystallographic plane (Poldervaart and Hess 1951). The subophitic clasts also vary with respect to degree of roundedness: the acicular plagioclase and medium-grained subophitic clasts are subangular, while the coarse-grained subophitic clasts are subrounded to rounded (Table 1), suggesting varied degrees of regolith mixing for different clast groups (Mittlefehldt et al. 2013).

Granoblastic Clasts

The granoblastic-textured clasts show variations in angularity, size, and grain size (Table 1). The overall texture of this type of clasts is indicative of recrystallization due to thermal metamorphism, with prevalent triple junctions between silicate grains (Yamaguchi et al. 1996). Most granoblastic clasts have a fine-grained texture (Fig. 3A), but also include medium- (similar to Emmaville; Yamaguchi et al. 1996) and coarse-grained (Fig. 3B) examples. The relative grain sizes likely are the product of initial grain size and degree of thermal metamorphism. The mineral proportions are approximately the same in the coarser-grained clasts relative to finer-grained granoblastic clasts. Additionally, the mineral modal abundances of the granoblastic clasts are indistinguishable from the subophitic clasts (Table 1). One group of fine granoblastic clasts shows remnant lath-shaped plagioclase crystals (Fig. 3A), similar to Agoult (Yamaguchi et al. 2009), suggesting a relatively lower degree of thermal metamorphism. Exsolution lamellae in pyroxene of the granoblastic clasts are fine (<1–40 μm) and appear to follow a single crystallographic orientation in each grain. Fine granoblastic clasts differ from the coarse granoblastic clasts in that they are angular to subangular, with one of the clasts having a distinct rectangular shape, while coarse clasts are rounded.

Cumulate Eucrite Clasts

A single subrounded cumulate eucrite clast was identified in this sample (Fig. 4), distinguished by its Mg-rich pyroxene, high modal abundance of plagioclase, cumulate texture, and pyroxene exsolution (Takeda 1997). The overall texture consists of subhedral pyroxene with interstitial plagioclase and silica as two large lath-shaped crystals (Table 1). This texture suggests relatively slow cooling and crystallization in an intrusive body (Yamaguchi et al. 2001). The pyroxenes exhibit exsolution lamellae similar to those observed in other eucritic clasts in NWA 5232 with high-Ca exsolution lamellae <1–20 μm in width, frequently offset along fractures. The exsolution texture displayed by the pyroxene in this clast would be described as Moore County type with thick parallel augite lamellae, rather than blebby augite, as in Binda (Takeda 1997). Chromite is the most abundant of the accessory phases in this clast and is typically within or in contact with pyroxene and is overgrown by ilmenite on the side of the grain in contact with plagioclase, and troilite is present as rare round <5 μm inclusions in pyroxene. The overall texture and exsolution lamellae of this clast are similar to those described in other HED polymict breccias (e.g., ALHA80102; Treiman and Drake 1985) and cumulate eucrites (e.g., Moore County; Hess and Henderson 1949), though the NWA 5232 cumulate clast is finer in grain size than Moore County (e.g., pyroxene in NWA 5232 are less than 1 mm in size, whereas those in Moore County generally range from 2 to 2.5 mm) and has relatively fine lamellae (<20 μm versus 25–100 μm in Moore County).

Pyroxene-Lath Clasts

A single clast comprises pigeonite laths surrounded by plagioclase and augite (Fig. 5). This fine-grained clast is angular and rectangular in shape (Table 1) and has significant Fe-staining visible in both thin section and hand sample, likely due to the presence of Fe-Ni metal. It is the only eucritic clast present in NWA 5232 that lacks pyroxene exsolution lamellae resolvable with EMP. Pigeonite crystals are euhedral to subhedral, tabular to lath-shaped, and show no preferred orientation. A bimodal population of pigeonite crystals is present: the larger pigeonite crystals are more tabular and contain fine opaque inclusions, while the smaller pigeonite crystals are lath like and lack inclusions. In BSE, all pyroxene grains lack any evidence of exsolution lamellae, but pigeonite laths and some augite crystals show faint compositional zoning, with relatively Ca-poor rims. Augites are interstitial to the pigeonite and in places have overgrown pigeonite laths. This pyroxene-lath clast is the only eucritic clast in NWA 5232 that contains no silica. The pyroxene-lath texture is indicative of rapid cooling, and the presence of larger, likely relict, pyroxene grains suggests that this clast is an impact melt clast.

Olivine-Rich Clast

The most petrographically distinct clast type is the olivine-rich clast, which is represented by a single clast in the 42 clasts examined in detail (Fig. 6). This clast shows a nonuniform distribution of mineral constituents and is distinct in its lack of plagioclase and significant proportion of fayalitic olivine (Fo_{15}) (Table 1). Pyroxene shows fine exsolution lamellae and high-Ca regions within grains. There is a concentration of

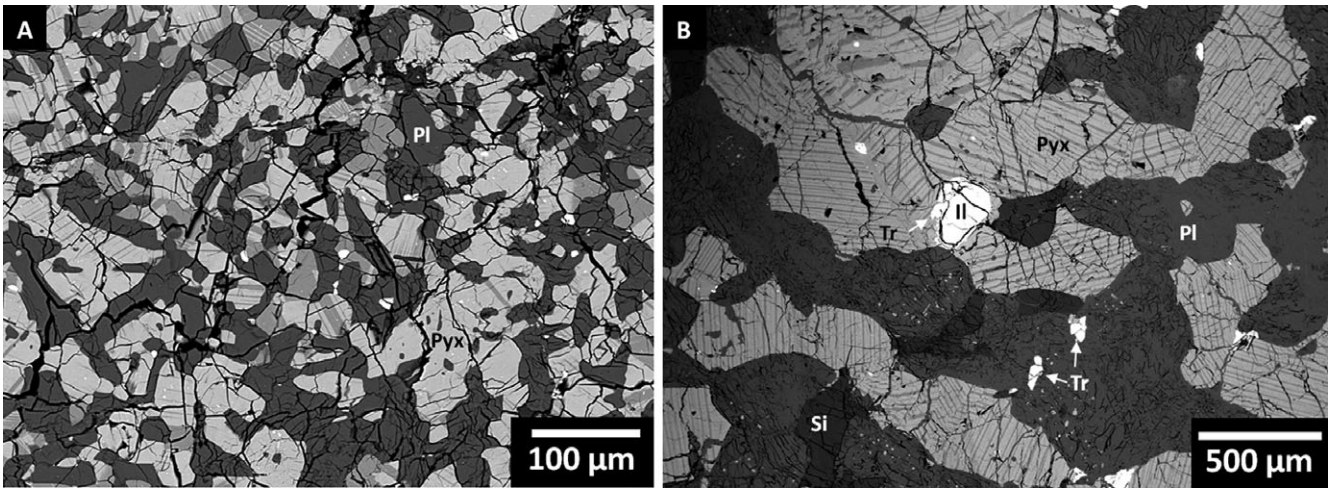

Fig. 3. BSE images of granoblastic clasts. The silicates in these clasts are plagioclase (Pl), pyroxene (Pyx), and silica (Si); the white phases are ilmenite (Il) and troilite (Tr). A) Finer granoblastic-textured clast with remnant subophitic texture (plagioclase laths) similar to that observed in Agoult (Yamaguchi et al. 2009). B) Coarse granoblastic-textured clast.

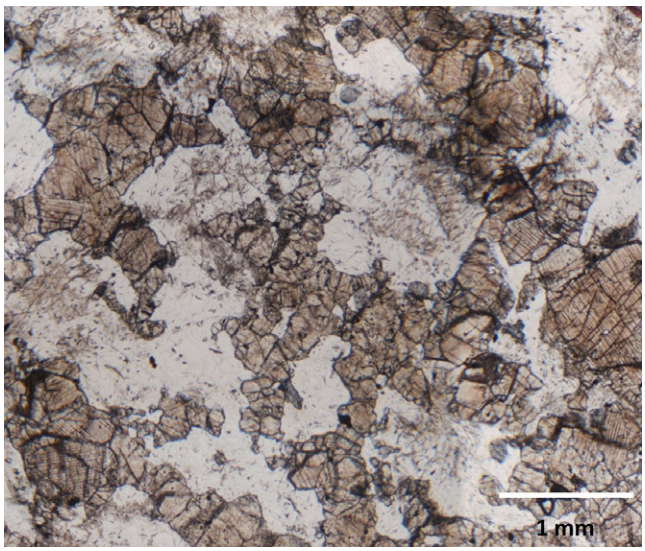

Fig. 4. Plane polarized light (PPL) photomicrograph of the cumulate eucrite clast. The brown mineral is pyroxene, and the transparent mineral is primarily plagioclase. This texture is similar to that in Moore County (Hess and Henderson 1949).

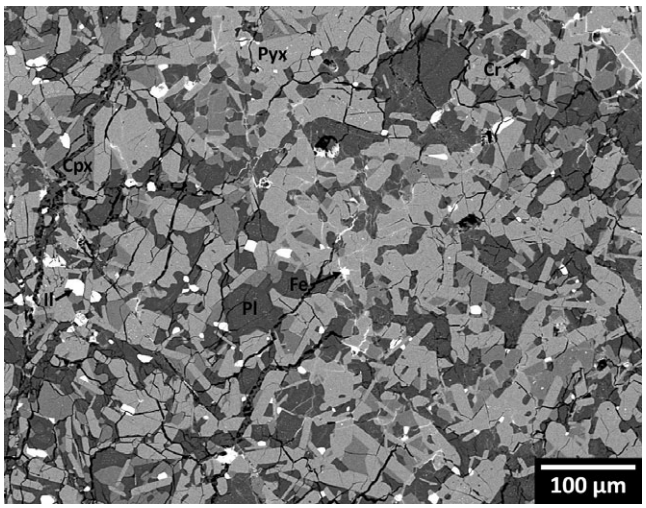

Fig. 5. BSE image of pyroxene-lath clast. The silicates in these clasts are low-Ca pyroxene (Pyx), high-Ca pyroxene (Cpx), and plagioclase (Pl). The white phases are ilmenite (Il), chromite (Cr), and Ni-Fe metal (Fe). The presence of Ni-Fe metal may be contamination from an impactor.

ilmenite on one end of the clast, primarily as a single 500 × 300 µm grain next to an irregular vermicular intergrowth of ilmenite and pyroxene. The intergrowth in this olivine-rich clast is similar to the symplectites in howardites reviewed by Patzer and McSween (2012) and Barrat et al. (2012). Three-stage symplectite intergrowths involving fayalitic olivine, Fe-rich pyroxene, and silica are interpreted to represent late-stage melt evolution as a breakdown product of a quickly cooled Fe-rich metastable pyroxene, pyroxferroite (Lindsley and Burnham 1970; Barrat et al. 2012; Patzer and McSween 2012). The olivine-rich clast in NWA 5232 is significantly different from the olivine-bearing clasts and mineral fragments in howardites described by Beck et al. (2012) in that the clast in NWA 5232 contains olivine that are significantly more Fe rich and lack compositional zoning.

Breccia Clasts

The breccia clasts are a significant clast type present in NWA 5232 (Fig. 1). Their textures are quite variable and comprise individual crystal fragments with minor eucritic clasts or impact melt clasts. No breccia clasts

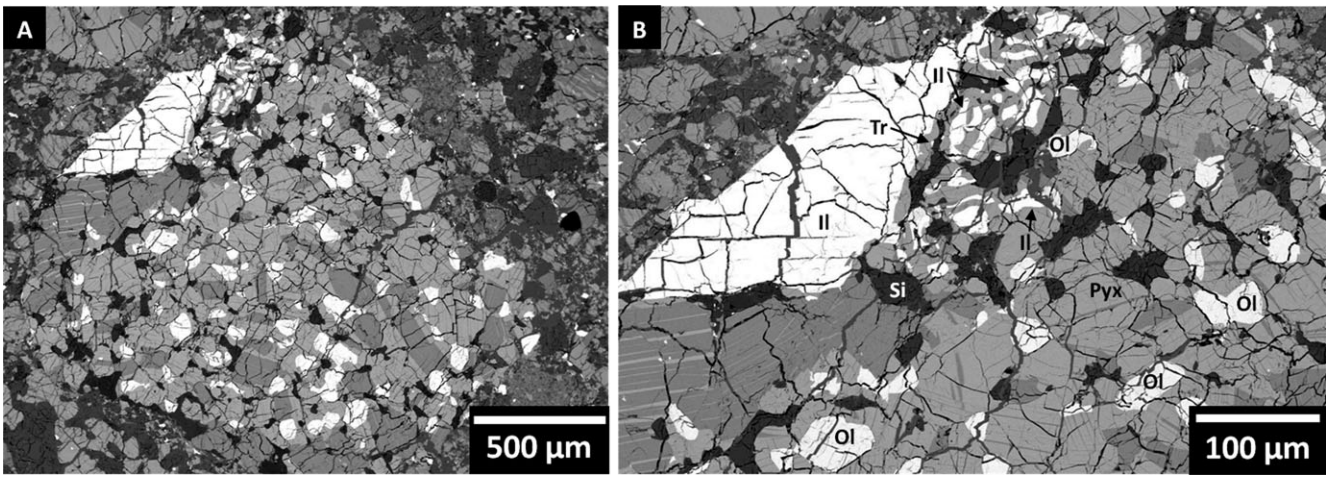

Fig. 6. BSE image of olivine-rich clast. Light gray is pyroxene (with darker high-Ca pyroxene) (Pyx), dark gray is silica (Si), and white phases are fayalitic olivine (Ol), ilmenite (Il), and trace troilite (Tr). A) Olivine-rich clast surrounded by matrix. B) Intergrowth of ilmenite and Fe-rich pyroxene in the same olivine-rich clast.

were observed to contain carbonaceous chondrite material. The clasts are generally subrounded and range in size from 0.5 to 24 mm. They consist of mineral fragments compositionally and texturally similar to those observed in other eucritic clasts, including pyroxene with exsolution lamellae. The clasts are well indurated and exsolution lamellae are commonly bent, likely due to shock. Mineral fragments are highly fractured, containing fractures that are both restricted to individual mineral grains (predate consolidation as a breccia clast) and those that continue through adjacent mineral fragments (postdate consolidation). In appearance, they resemble the matrix of NWA 5232, but are distinguished by their color (light brown) and the recrystallized nature of intraclast matrix (Fig. 7). These clasts have been identified in other HED polymict breccias (e.g., Delaney and Prinz 1984) and are an important constituent as they attest to the complex and multi-stage mixing history of NWA 5232 (Pun et al. 1998).

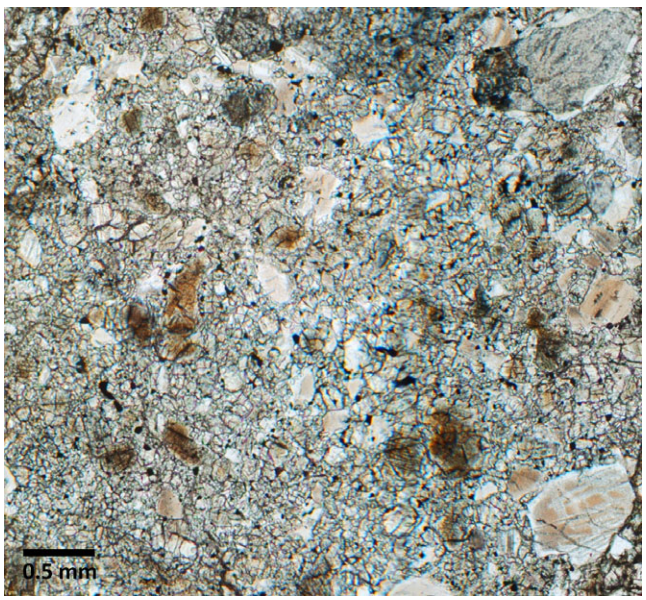

Fig. 7. PPL photomicrograph of breccia clast. This clast consists of a heterogeneous mixture of fragments of eucritic material and matrix from a previous generation of breccia.

Clast Comparisons

The crystallization textures of the clasts indicate a diverse cooling (and reheating) history of the individual lithologies sampled by this breccia. Textures exhibited by clasts such as the acicular subophitic and pyroxene-lath clasts suggest rapid crystallization and may indicate cooling closer to the surface of the EPB. However, the acicular subophitic clasts still show pyroxene exsolution lamellae, indicative of secondary reheating (Takeda and Graham 1991). All of the eucritic clasts in NWA 5232 experienced secondary thermal metamorphism prior to incorporation into the regolith mixture, as observed in other polymict eucrites (e.g., Delaney and Prinz 1984), though to different degrees, from the pyroxene-lath clasts, which retain compositional zoning, to the coarse-grained granoblastic clasts, which show extensive recrystallization and pyroxene exsolution lamellae. All of the subophitic and granoblastic clasts would be categorized as type 4–5 (Takeda and Graham 1991) and described as ordinary eucrites (Takeda 1991). Within the broad textural types, systematic differences were noted between clast groups with respect to clast rounding (i.e., clasts of the same group show the same

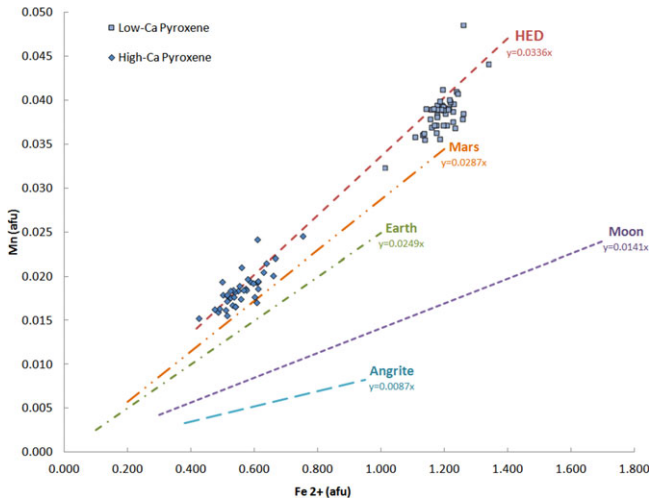

Fig. 8. A total of 399 pyroxene data points for 42 individual igneous-textured clasts were obtained for NWA 5232; this is a plot of average low- and high-Ca pyroxene compositions for each clast. The data plot along the HED line (trend lines from Papike et al. 2003).

degree of mechanical rounding). For example, the coarse-grained granoblastic clasts were well-rounded compared with the angular-subangular finer-grained granoblastic clasts.

Eucritic Clast Mineral Compositions

As a regolith breccia, NWA 5232 contains a variety of clast types, both derived from its parent asteroid and exogenic clasts (e.g., carbonaceous chondrite clasts). As a consequence of this, it is important to determine the parentage of the individual clasts studied. The method described by Papike et al. (2003) of determining the Mn/Fe of pyroxene by electron microprobe to distinguish the planetary body origin of basaltic meteorites is an effective and accessible means of establishing clast origin. Average compositions of low-Ca and high-Ca pyroxenes for each clast were plotted on a Fe versus Mn (atoms per formula unit, afu) plot, illustrating their HED parentage (Fig. 8). Much of the NWA 5232 data plot below the line of expected HED compositions, but this line is an average of unequilibrated eucrites and diogenites (Papike et al. 2003); if unequilibrated eucrites alone are plotted, the slope of this reference line would decrease toward the majority of NWA 5232 data points (Papike 1998). One clast shows a higher Mn (afu) composition, plotting above the HED reference line; this is a single small (0.8 mm) rust-stained pyroxene-dominated clast (low-Ca pyroxene average $Wo_{2.4}Fs_{63.9}En_{33.7}$ and plagioclase average $An_{88.4}$) with minor Fe-metal veins and accessory silica, chromite, and ilmenite. All other igneous clasts examined in NWA 5232 fall along the HED line of Mn/Fe.

Pyroxene Compositions

Eucritic clast pyroxene major elements have been plotted by texture on the pyroxene quadrilateral (Fig. 9). Both the subophitic- and granoblastic-textured eucritic clasts, the most abundant clast types in NWA 5232, plot within the basaltic eucrite field by pyroxene major element compositions (Takeda 1997). These clast types have average low-Ca pyroxene values ranging from $En_{32–40}$ (Figs. 9A–E; Table 2). The most Mg-rich clast type is the cumulate-textured clast, and the most Mg-poor clast is the olivine-rich clast type (Fig. 9F; Table 2). No diogenitic clasts or crystal fragments in the matrix were observed.

Major element compositions are equilibrated within individual clasts, as indicated by the limited variation in low-Ca En values. Pyroxene quadrilateral composition trends have been described by Pun and Papike (1996), who outline three trends of chemical zoning and exsolution; all basaltic eucrite clasts in NWA 5232 follow the Fe-Ca trend of tie-lines from host pigeonite with exsolved augite and are ordinary eucrites (Takeda and Graham 1991). Intermediate compositions between low- and high-Ca pyroxene are likely the consequence of electron microprobe beam overlap of exsolved lamellae and host pyroxene (e.g., Pun and Papike 1996).

The pyroxene compositions of the cumulate clast are the most Mg rich in NWA 5232 (Table 2), but relative to other cumulate eucrites are high in Fe, with slightly lower Mg# than Moore County (Mg# 47.7 compared with 48.6 for Moore County; Pun and Papike 1995). The overall and pyroxene exsolution textures of the Mg-rich clast in NWA 5232 (Fig. 4) are also similar to Moore County (Hess and Henderson 1949). The NWA 5232 cumulate clast is more Mg rich than the unusual Pomozdino eucrite (Mg# 46.4), described as a partial cumulate eucrite, and has a distinctly different texture (Warren et al. 1990).

The En compositions of low-Ca pyroxene within individual clasts (and clast groups) are not tightly restricted in some clast types, such as the Mg-rich coarse-grained subophitic clasts (Fig. 9B), which show an En range of 4.3. Conversely, some clast types show a tight grouping of low-Ca pyroxene compositions, such as the lower-Mg fine-grained subophitic clast group (Fig. 9A), which show an En range of 0.8. This variation in the range of low-Ca major element compositions suggests a variation in the degree of either slow cooling processes or secondary thermal equilibration of these clasts (Pun and Papike 1996).

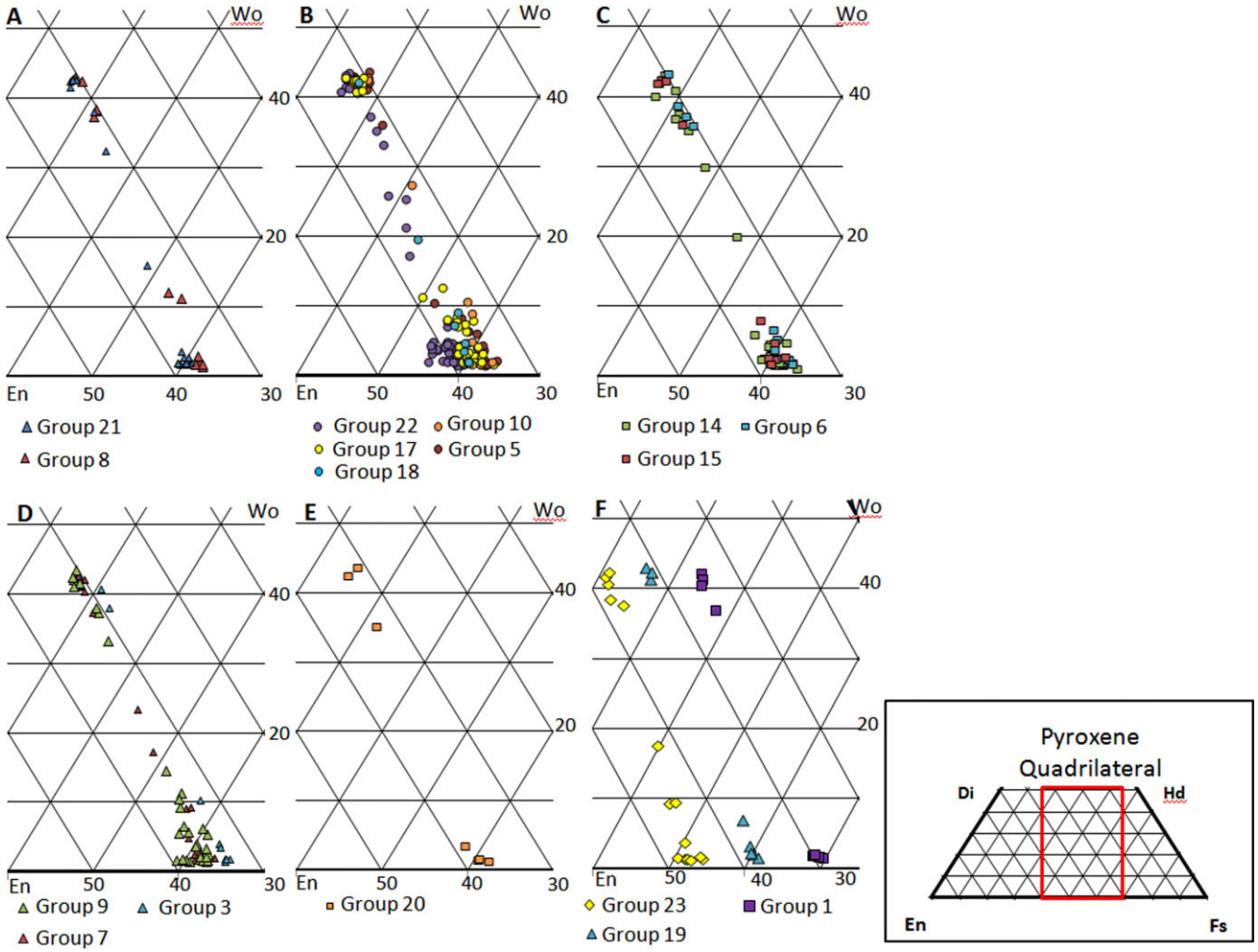

Fig. 9. Sections of pyroxene quadrilateral with eucritic clast compositions plotted by textural type. Twenty distinct types of eucritic clast (defined by texture and pyroxene compositions) have been noted in NWA 5232, plotted in groupings by texture (excluding single crystal and breccia clasts). Red box on pyroxene quadrilateral indicates section plotted here. A) Acicular subophitic (e.g., Fig. 2A); B) coarse-grained subophitic (e.g., Fig. 2B); C) medium-grained subophitic; D) fine- and medium-grained granoblastic (e.g., Fig. 3A); E) coarse-grained granoblastic (e.g., Fig. 3B); and F) in order of decreasing Mg content, cumulate (Fig. 4), pyroxene lath (Fig. 5), and olivine rich (Fig. 6).

Most of these clast types are similar in composition and texture to those described by others from howardites, polymict eucrites, and monomict eucrites (e.g., Pun et al. 1998; Patzer et al. 2005; Mayne et al. 2009). The most unusual clast type observed in NWA 5232 is the olivine-rich clast (Fig. 6), which consists of fayalitic olivine, Fe-rich pyroxene, silica, and ilmenite (Table 1). The olivine compositions are Fe rich throughout the clast ($Fo_{14.1–15.2}$), and pyroxene has the lowest Mg content of all the eucritic clasts reviewed in this study (Fig. 9F; Table 2).

Minor element compositions of eucritic clast pyroxene are plotted in Fig. 10. This is a small sample of clast types measured, but they were chosen to illustrate the variety of minor element trends observed in clasts and to be representative of the general clast texture types. Most clasts are equilibrated with respect to minor elements (plot as tight clusters), but crystallization trends can still be resolved (Mayne et al. 2009).

Two main crystallization trends can be inferred from these minor element ternary plots (1) early crystallization of pyroxene before the onset of plagioclase crystallization and (2) crystallization of pyroxene before plagioclase reached the solidus (Pun and Papike 1996; Mayne et al. 2009). These trends are primarily the result of three substitution couples: $^{VI}Cr^{3+}$-$^{IV}Al^{3+}$, $^{VI}Al^{3+}$-$^{IV}Al^{3+}$, and $^{VI}Ti^{4+}$-$2^{VI}Al^{3+}$ (Papike 1998). For the trend 1 crystallization sequence, basaltic assemblages begin at Cr-rich pyroxene

Table 2. Representative mineral analyses for eucritic clasts in polymict eucrite NWA 5232.

	Cumulate			Subophitic acicular		Subophitic coarse			Pyroxene lath		Granoblastic		Olivine-rich		
	Low-Ca Pyx	High-Ca Pyx	Plag	Low-Ca Pyx	High-Ca Pyx	Low-Ca Pyx	High-Ca Pyx	Plag	Low-Ca Pyx	High-Ca Pyx	Low-Ca Pyx	High-Ca Pyx	Low-Ca Pyx	High-Ca Pyx	Olivine
SiO_2	50.8	50.9	45.6	49.7	50.2	49.8	51.1	45.2	50.0	51.6	48.8	50.9	49.0	50.1	31.5
Al_2O_3	0.26	1.48	35.3	0.12	1.28	0.29	0.63	35.7	0.11	0.45	0.43	0.41	0.14	0.84	0.01
MgO	15.8	12.4	0.03	12.9	10.1	12.3	10.4	0.01	12.5	10.5	11.8	10.2	9.61	8.27	6.10
FeO	31.1	12.8	0.17	35.0	16.2	36.1	16.5	0.07	35.4	15.2	36.3	16.9	39.0	20.0	60.8
CaO	0.69	20.7	17.9	0.89	20.7	0.89	20.3	18.3	0.95	21.1	1.13	20.5	0.97	19.4	0.06
MnO	0.96	0.47		1.02	0.58	1.15	0.54		1.02	0.52	1.16	0.52	1.34	0.58	1.47
Cr_2O_3	0.28	0.36		<0.05	0.23	0.06	0.33		<0.05	0.19	0.13	0.19	0.06	0.27	0.02
K_2O	<0.02	<0.02	0.09	<0.02	<0.02	<0.02	<0.02	0.06	<0.02	<0.02	<0.02	<0.02	<0.02	<0.02	<0.02
Na_2O	<0.03	0.06	1.06	0.05	<0.03	<0.03	0.09	1.04	<0.03	0.08	<0.03	0.04	<0.03	0.09	<0.03
TiO_2	0.21	0.74		0.14	0.70	0.07	0.34		0.07	0.32	0.33	0.25	0.12	0.44	0.06
Total	100.05	99.84	100.09	99.89	100.07	100.66	100.24	100.34	99.92	99.93	100.14	99.95	100.21	99.94	99.97
Si	1.98	1.94	2.15	1.98	1.94	1.98	1.96	2.14	1.99	1.98	1.96	1.97	1.99	1.96	1.01
Al	0.01	0.07	1.97	0.01	0.06	0.01	0.03	1.99	0.01	0.02	0.02	0.02	0.01	0.04	0.00
Mg	0.92	0.70	0.00	0.77	0.58	0.73	0.60	0.00	0.74	0.60	0.71	0.59	0.58	0.48	0.29
Fe^{2+a}	1.01	0.39	0.01	1.17	0.51	1.20	0.53	0.00	1.18	0.49	1.22	0.55	1.32	0.64	1.63
Fe^{3+}	0.00	0.02		0.00	0.01	0.00	0.01		0.00	0.00	0.00	0.00	0.00	0.01	
Ca	0.03	0.84	0.68	0.04	0.86	0.04	0.83	0.70	0.04	0.87	0.05	0.85	0.04	0.81	0.00
Mn	0.03	0.02		0.03	0.02	0.04	0.02		0.03	0.02	0.04	0.02	0.05	0.02	0.04
Cr	0.01	0.01		0.00	0.01	0.00	0.01		0.00	0.01	0.00	0.01	0.00	0.01	0.00
K	0.00	0.00	0.00	0.00	0.00	0.00	0.00	0.00	0.00	0.00	0.00	0.00	0.00	0.00	0.00
Na	0.00	0.00	0.10	0.00	0.00	0.00	0.01	0.10	0.00	0.01	0.00	0.00	0.00	0.01	0.00
Ti	0.01	0.02		0.00	0.02	0.00	0.01		0.00	0.01	0.01	0.01	0.00	0.01	0.00
Total	4.00	4.00	4.91	4.01	4.01	4.00		4.92	4.00	4.00	4.01	4.01	4.00	4.00	2.97
En/Fo[b]	46.9	37.4		38.9	30.6	37.0			37.8	31.4	35.7	29.9	29.8	25.4	15.2
Fs/Fa[b]	51.6	20.8		59.1	26.9	61.1			60.1	25.5	61.8	27.8	68.0	34.0	84.8
Wo	1.5	41.8		1.9	42.5	1.9			2.1	43.1	2.5	42.2	2.2	40.6	
Mg#	47.7	63.1		39.7	52.7	37.8	52.6		38.5	55.0	36.8	51.8	30.5	42.5	
An			87.1					87.7							
Ab			12.4					12.0							
Or			0.5					0.3							

Pyroxene (Pyx) calculated per 6 oxygen, plagioclase (Plag) per 8 oxygen, and olivine per 4 oxygen. [a]Pyroxene data corrected for Fe^{3+}; where no Fe^{3+} value given, Fe^{2+} is Fe_{Total}. [b]Values are for ether pyroxene or olivine, were appropriate. Mg# = $Mg/(Mg + Fe^{2+} + Fe^{3+}) \times 100$ calculated for pyroxene compositions.

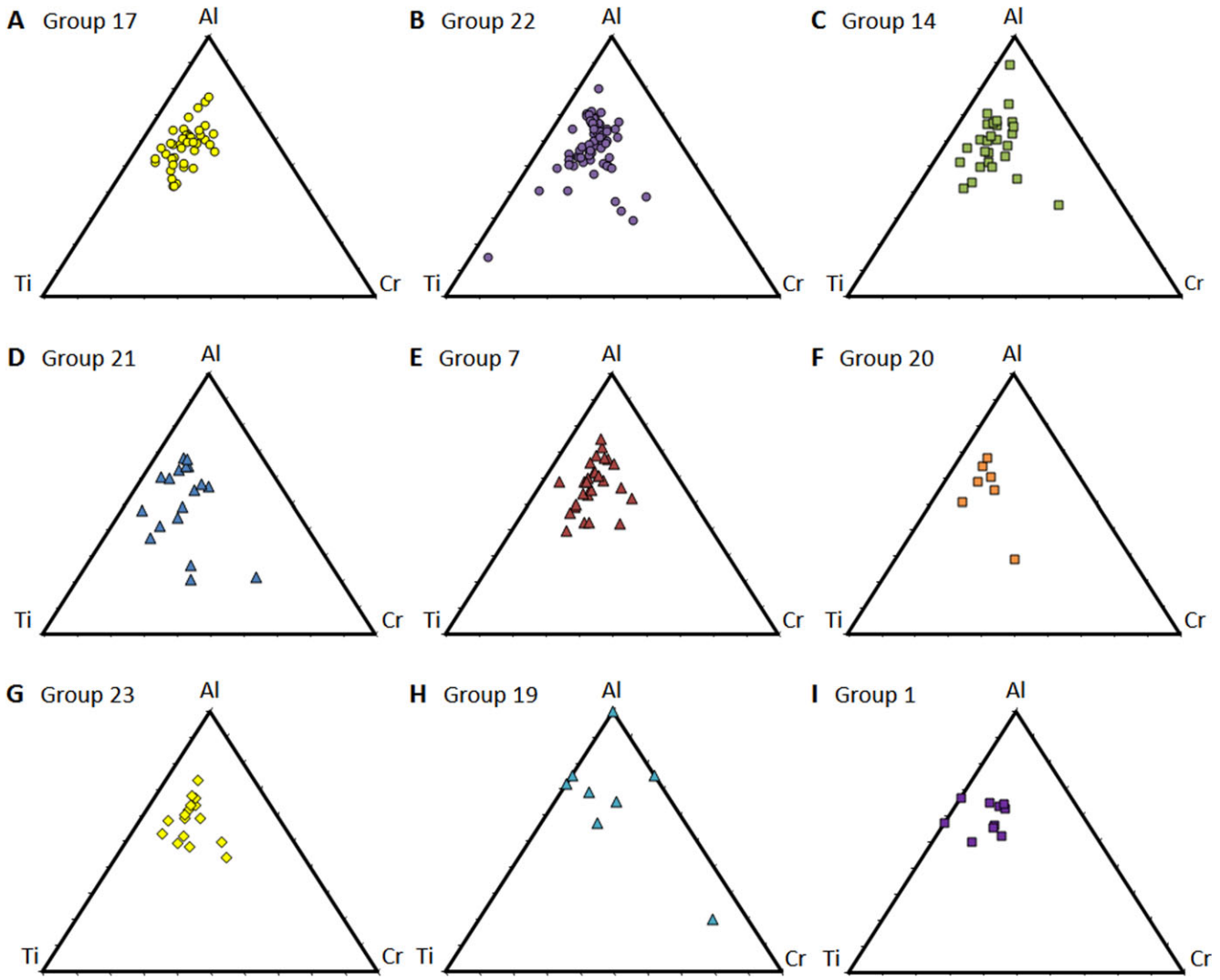

Fig. 10. Sample pyroxene minor element plots for the textural types of eucritic clasts in NWA 5232. These are the same groupings as in Fig. 9. A, B) Coarse-grained subophitic, C) medium-grained subophitic, D) acicular subophitic, E) fine-grained granoblastic, F) coarse-grained granoblastic, G) cumulate, H) pyroxene lath, and I) olivine rich.

compositions and become increasingly Al rich as Cr is removed from the melt, shifting from the $^{VI}Cr^{3+}$-$^{IV}Al^{3+}$ couple to the $^{VI}Al^{3+}$-$^{IV}Al^{3+}$ substitutional couple as Cr is depleted (Pun and Papike 1996; Mayne et al. 2009). Trend 2 crystallization represents a shift to the $^{VI}Ti^{4+}$-$2^{VI}Al^{3+}$ substitution couple as Al is taken up by plagioclase rather than just pyroxene (Mayne et al. 2009). Trend 2 appears to be the dominant trend represented by NWA 5232 clasts, as they primarily show variation in Ti and Al compositions with relatively little variation in Cr content of the pyroxene (Fig. 10). These trends must be interpreted with caution as the clustering of points is likely affected by equilibration of pyroxene compositions and exsolution of ilmenite and chromite during metamorphism (Yamaguchi et al. 2009). It is interesting to note that the minor element composition of the olivine-rich clast (Fig. 10I), which lacks plagioclase, shows a tight cluster of minor element compositions (a Cr-poor trend), which may allude to late-stage crystallization (Patzer and McSween 2012).

Plagioclase Compositions

Plagioclase compositions of basaltic achondrites typically have restricted values for An and potassium content (Papike et al. 2003). Plagioclase compositions for eucritic clasts in NWA 5232 are consistent with those for eucrites, which are typically calcic, ranging from bytownite to anorthite (Mittlefehldt et al. 1998). Compositions were determined for 11 clasts ($n = 94$) and clast averages range from $An_{86.3}$ to $An_{88.6}$ and K

Table 3. Oxygen isotopic compositions of clasts in NWA 5232.

Sample	Texture	$\delta^{17}O‰$	$\delta^{18}O‰$	$\Delta^{17}O‰$
Eucritic clasts				
NWA 5232_a	Subophitic—medium	1.73	3.81	−0.270
NWA 5232_d	Granoblastic—coarse	1.47	3.34	−0.283
NWA 5232_e	Subophitic—medium	1.86	4.03	−0.256
NWA 5232_f	Subophitic—coarse in breccia clast	1.80	3.87	−0.242
NWA 5232_g	Granoblastic—fine	1.55	3.39	−0.232
NWA 5232_h	Breccia	1.85	3.98	−0.245
NWA 5232_i	Subophitic—medium	1.65	3.57	−0.228
NWA 5232_j	Breccia	1.57	3.43	−0.239
NWA 5232-2	Subophitic—acicular	1.57	3.52	−0.287
NWA 5232-4	Subophitic—medium	1.56	3.56	−0.311
NWA 5232-6	Granoblastic—coarse	1.42	3.24	−0.281
NWA 5232-7	Granoblastic—fine	1.57	3.49	−0.267
NWA 5232-8	Subophitic—coarse	1.61	3.55	−0.260
NWA 5232-9	Impact melt (IM)	1.58	3.45	−0.236
NWA 5232-10	Pyx lath (IM)	1.59	3.36	−0.176
		1.65	3.39	−0.137
NWA 5232-12	Subophitic—medium	1.49	3.33	−0.261
NWA 5232	Bulk 1	1.67	3.65	−0.246
NWA 5232	Bulk 2	1.42	3.21	−0.270
Cumulate eucrite clast				
NWA 5232-11	Cumulate	1.60	3.47	−0.224
Carbonaceous chondrite clasts				
NWA 5232_b	Clast 1	−0.61	3.63	−2.519
NWA 5232_c	Clast 1	−2.27	3.02	−3.855
NWA 5232_k	Clast 2	−0.58	4.46	−2.929
NWA 5232	Bulk 3	−1.20	3.72	−3.154

Samples with a letter designation were powered samples extracted from slices by drill (locations shown in supporting information), samples with a number designation were crushed aliquots of clasts removed for multiple analyses, and bulk samples were taken of primarily eucritic and carbonaceous chondrite material, respectively, for initial work.

(afu) contents of 0.003–0.005, well within the expected values for these meteorites (Table 2). Plagioclase lacks compositional zoning but showed compositional variation between grains within clasts (see supporting information); this compositional variation is most strongly pronounced in the subophitic-textured clasts. The plagioclase in the cumulate clast is less calcic ($An_{87.1}$) than would be anticipated for a cumulate eucrite, typically $An_{91–95}$, and is less calcic than Moore County ($An_{91.3}$; Mittlefehldt et al. 1998) but more calcic than Pomozdino ($An_{85.6}$; Warren et al. 1990).

Carbonaceous Chondrite Clasts

In addition to eucritic clasts, exogenic carbonaceous chondrite clasts are present as dark material (Fig. 1). Carbonaceous chondrite clasts are black in color with minor iron staining, range in size from 0.1 mm to 1 cm, are generally angular to subangular in shape, and are distributed irregularly throughout the meteorite. The carbonaceous chondrite clasts have irregular boundaries with the eucritic matrix and, in places, show minor disaggregation and localized mechanical mixing of dark clast fragments mixed into the eucritic matrix (see supporting information).

The carbonaceous chondrite clasts are similar to material described in other HED polymict breccias (e.g., Zolensky et al. 1996) as CM clasts. The clasts consist of aggregates, containing ferromagnesian silicates and sulfides, supported by a fine-grained matrix. These aggregates are most commonly elliptical or irregular in shape, average 300 μm in size (up to 1 mm), and are predominantly surrounded by dust rims, a feature commonly observed in CM carbonaceous chondrites (Metzler et al. 1992). Crystal fragments and rare round chondrules can be observed in these clasts. P-rich Fe-Ni-sulfide was identified in numerous aggregates in all carbonaceous chondrite clasts examined, a phase that is characteristic of CM carbonaceous chondrites (Nazarov et al. 2009).

Oxygen Isotopes

Oxygen isotope analyses were conducted on 21 individual clasts, 18 light-colored and 3 black fine-grained clasts, plus 3 bulk samples extracted from slices of NWA 5232 (Table 3). The eucrite and diogenite meteorites have whole-rock $\delta^{18}O$ values ranging from 3.0 to 4.2‰; their $\Delta^{17}O$ values, however, are restricted to a very narrow range of values, $-0.242 \pm 0.004‰$ (Greenwood et al. 2005; Wiechert et al. [2004] have a different calibration for $\Delta^{17}O$ but report a similarly narrow range of values). Diogenites are orthopyroxenites (and dunites, see Beck et al. 2011) with $\delta^{18}O$ values that lie at the low end of the range. Eucrites are basaltic, with clinopyroxene–plagioclase assemblages; their $\delta^{18}O$ values are at the high end of the range. The eucritic matrix (please see sample description in the Methods section) and clasts of NWA 5232 range in $\delta^{18}O$ from 3.2 to 4.0‰ but have a small range in $\Delta^{17}O$, i.e., $-0.25 \pm 0.04‰$ (Table 3). Petrographic observations and chemical data document the occurrence of subophitic and granoblastic eucritic lithologies. A striking observation is that the granoblastic-textured clasts examined in NWA 5232 tend to have lower $\delta^{18}O$ values relative to the subophitic-textured clasts, although the relative abundances of pyroxene and plagioclase in these clasts are within the same range and pyroxene major element compositions of both of these clast types are within the range of basaltic eucrites (Fig. 11). The lower $\delta^{18}O$ of the granoblastic clasts may reflect the variable sampling of the clasts, as the lowest $\delta^{18}O$ values are for the coarse granoblastic samples, which may have sampled

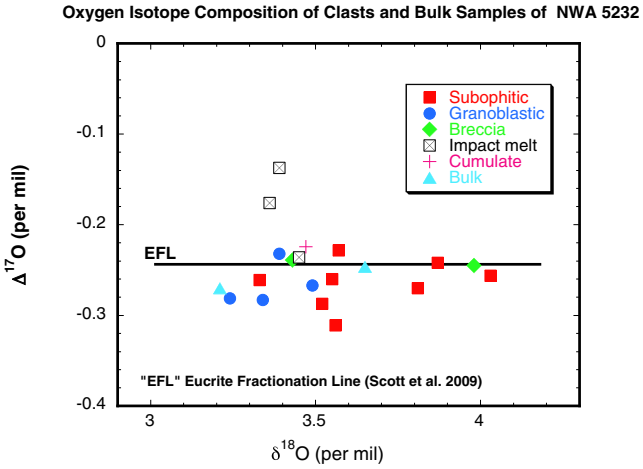

Fig. 11. Oxygen isotope compositions of NWA 5232 lithic clasts. The clasts show a small range in $\Delta^{17}O$, concentrated along the EFL. The pyroxene lath-textured clast (the two impact melt data points with high $\Delta^{17}O$ values) are well removed from this line, suggesting origin or contamination by exogenic sources. The granoblastic- and subophitic-textured clasts have distinct $\delta^{18}O$ ranges.

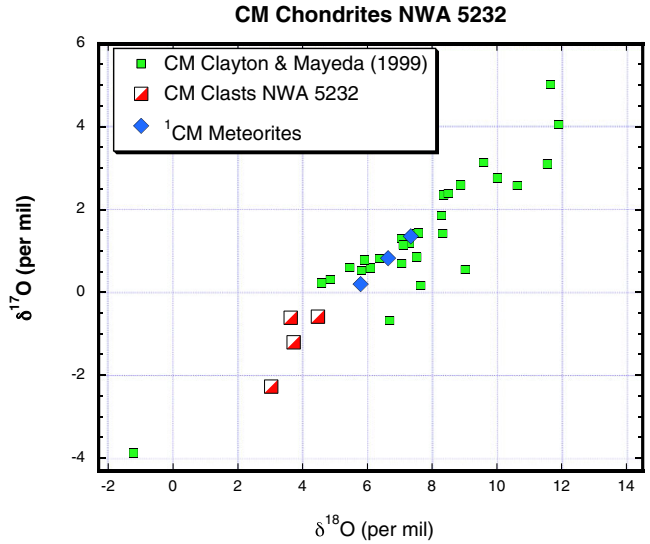

Fig. 12. Carbonaceous chondrite clast compositions from NWA 5232 plotted with CM compositions from Clayton and Mayeda (1999), LAP 02277 and MET 01070 (Moriarty et al. 2009), and NWA 3340 (corrected data Meteoritical Bulletin Database). Compositions of CM meteorites that plot in the lower-left part of the diagram indicate a less pronounced aqueous alteration contribution to the oxygen isotopic ratios.

more pyroxene relative to plagioclase. However, no correlation exists between clast grain coarseness and $\delta^{18}O$ values for the subophitic-textured clasts, so this explanation seems less likely. The range in $\delta^{18}O$ of clasts and matrix of NWA 5232 reflects its origin as a breccia of mixed clasts dominated by eucritic rock types, including two breccia clasts, one of which contains a large subophitic clast (NWA 5232_h contains subophitic NWA 5232_f).

The extreme values of $\Delta^{17}O$, $-0.16 \pm 0.03‰$ for NWA 5232-10 (pyroxene lath) and $-0.31‰$ for NWA 5232-4 (subophitic medium), may indicate derivation or contribution from separate parent bodies (Scott et al. 2009). Since the pyroxene major elements and Mn/Cr values are consistent with HED meteorites, the pyroxene-lath clast is likely an impact melt clast that variably incorporated material from an impactor with a higher value for $\Delta^{17}O$ rather than entirely being an exogenic clast. Clast NWA 5232-4 pyroxene has major element and Mn/Cr values that are consistent with HED meteorites and the subophitic texture is typical of other eucritic clasts, so further work is required to establish if this clast is exogenic or an anomalous eucrite.

The black fine-grained clast oxygen isotope compositions are consistent with CM carbonaceous chondrites (Table 3). The carbonaceous chondrite clasts of NWA 5232, with values of 3.0–4.5‰, lie at the low $\delta^{18}O$ end of the range of CM chondrites (Fig. 12), suggesting less aqueous alteration than observed in other CM chondrites (Rubin et al. 2007). The large range in $\delta^{18}O$ in CM clasts is caused by variable proportions of matrix, chondrules, and anhydrous silicate minerals in samples obtained by drilling. The CM chondrite clasts of NWA 5232 are fragments of bolides that impacted the eucrite-diogenite parent body and it is reasonable that other foreign material was incorporated, a possible explanation for samples NWA 5232-4 and -10.

CONCLUSION

The main goal of this study was to establish the diversity of clast types represented in HED polymict breccia NWA 5232. Eucritic clasts were grouped on the basis of their texture, grain size, relative proportions of major and minor mineral constituents, pyroxene compositions, and plagioclase compositions. All lithic clasts reviewed were eucritic, and no diogenitic material was identified, supporting the classification of NWA 5232 as a polymict eucrite. Most eucritic clasts in NWA 5232 fall within the basaltic eucrite category, based on silicate compositions and textures, and show evidence of varying degrees of thermal metamorphism and shock (e.g., granoblastic textures, exsolution lamellae, and melt veins). The six general textural types observed in NWA 5232 can be further subdivided on the basis of composition and proportions of mineral constituents into 20 distinct groups (Fig. 9). It is unlikely that all of these groups represent different distinct lithologies or sources of material from the EPB, but rather may

represent sampling of larger scale heterogeneity, varied cooling rates, and secondary metamorphism. The clast groups with the largest number of individual clasts within NWA 5232 are the Mg-rich coarse-grained subophitic group (Fig. 9B—Group 22) and the Mg-rich fine-grained subophitic group (Fig. 9A—Group 21) with seven clasts (including single-crystal clasts with identical compositions) and four clasts, respectively. The cumulate-textured clast in NWA 5232 is a cumulate eucrite clast with unusually Fe-rich pyroxene and Ca-poor plagioclase, most closely resembling Moore County in pyroxene composition and texture.

The oxygen isotopic ratios determined for the eucritic clasts support the identification of eucritic lithologies present in NWA 5232, as suggested by petrographic and silicate composition review, as well as CM carbonaceous chondrite clasts. A systematic difference in $\delta^{18}O$ values between granoblastic and subophitic-textured clasts was identified, although the relative proportions of plagioclase and pyroxene are indistinguishable for these textures. The low $\delta^{18}O$ values measured for the CM clasts suggest that these clasts experienced a low degree of aqueous alteration prior to incorporation into the NWA 5232 regolith. Within the context of the EPB, likely 4 Vesta, NWA 5232 provides important insight into the impact processes and extent of mixing of eucritic and exogenic material on the surface of this asteroid.

Acknowledgments—The authors thank the reviewers and associate editor for their invaluable suggestions for improvements to this article. The authors also thank David Gregory for his donation of NWA 5232 to the Royal Ontario Museum and Ian Nicklin and Brendt Hyde for their technical assistance. This research was possible with a Discovery Grant from the Natural Sciences and Engineering Research Council of Canada (KTT), H. V. Ellsworth Graduate Fellowship in Mineralogy (KV), Gale Ruckledge Graduate Scholarship (KV), and Explorer's GSEF Scholarship (KV). Rumble thanks A. J. Irving (University of Washington) and Ian Nicklin (Royal Ontario Museum) for introducing him to NWA 5232. Expenses of oxygen isotope analyses were supported by NASA grant NNX07AI48G (DR).

Editorial Handling—Dr. Akira Yamaguchi

REFERENCES

Barrat J. A., Yamaguschi J. A., Bollinger C., and Boudouma O. 2012. Low-Mg rock debris in howardites: Evidence for KREEPy lithologies on Vesta? *Geochimica et Cosmochimica Acta* 99:193–205.

Beck A. W., Mittlefehldt D. W., McSween H. Y., Rumble D. III, Lee C. A., and Bodnar R. J. 2011. MIL 03443, a dunite from asteroid 4 Vesta: Evidence for its classification and cumulate origin. *Meteoritics & Planetary Science* 46(8):1133–1151.

Beck A. W., Welten K. C., McSween H. Y., Viviano C. E., and Caffee M. W. 2012. Petrologic and textural diversity among the PCA 02 howardite group, one of the largest pieces of the Vestan surface. *Meteoritics & Planetary Science* 47(6):947–969.

Binzel R. P., and Xu S. 1993. Chips off of asteroid 4 Vesta: Evidence for the parent body of basaltic achondrite meteorites. *Science* 260:186–191.

Bischoff A. and Stöffler D. 1992. Shock metamorphism as a fundamental process in the evolution of planetary bodies: Information from meteorites. *European Journal of Mineralogy* 4:707–755.

Cartwright J. A., Ott U., Mittlefehldt D. W., Herrin J. S., Herrmann S., Mertzman S. A., Mertzman K. R., Peng Z. X., and Quinn J. E. 2013. The quest for regolithic howardites. Part 1: Two trends uncovered using noble gases. *Geochimica et Cosmochimica Acta* 105:395–421.

Clayton R. N. and Mayeda T. K. 1999. Oxygen isotope studies of carbonaceous chondrites. *Geochimica et Cosmochimica Acta* 63:2089–2104.

Crozaz G., Floss C., and Wadhwa M. 2003. Chemical alteration and REE mobilization in meteorites from hot and cold deserts. *Geochimica et Cosmochimica Acta* 67:4727–4741.

Delaney J. S. and Prinz M. 1984. The polymict eucrites. *Journal of Geophysical Research* 89:C251–C288.

De Sanctis M. C., Ammannito E., Capria M. T., Tosi F., Capaccioni F., Zambon F., Carraro F., Fonte S., Frigeri A., Jaumann R., Magni G., Marchi S., McCord T. B., McFadden L. A., McSween H. Y., Mittlefehldt D. W., Nathues A., Palomba E., Pieters C. M., Raymond C. A., Russell C. T., Toplis M. J., and Turrini D. 2012. Spectroscopic characterization of mineralogy and its diversity across Vesta. *Science* 336:697–700.

Duke M. B. and Silver L. T. 1967. Petrology of eucrites, howardites and mesosiderites. *Geochimica et Cosmochimica Acta* 31:1637–1665.

Graham D. J. and Midgley N. G. 2000. Graphical representation of particle shape using triangular diagrams: An Excel spreadsheet method. *Earth Surface Processes and Landforms* 25:1473–1477.

Greenwood R. C., Franchi I. A., Jambon A., and Buchanan P. C. 2005. Widespread magma oceans on asteroidal bodies in the early solar system. *Nature* 435:916–918.

Hess H. H. and Henderson E. P. 1949. The Moore County meteorite: A further study with comment on its primordial environment. *American Mineralogist* 34:494–507.

Lindsley D. H. 1983. Pyroxene thermometry. *American Mineralogist* 68:477–493.

Lindsley D. H. and Burnham C. W. 1970. Pyroxferroite stability and X-ray crystallography of synthetic $Ca_{0.15}Fe_{0.85}SiO_3$ pyroxenoid. *Science* 168:364–367.

Liu Y., Floss C., Day J. M. D., Hill E., and Taylor L. 2009. Petrogenesis of lunar mare basalt meteorite Miller Range 05035. *Meteoritics & Planetary Science* 44:261–284.

Mayne R. G., McSween H. Y. Jr., McCoy T. J., and Gale A. 2009. Petrology of the unbrecciated eucrites. *Geochimica et Cosmochimica Acta* 73:794–819.

Metzler K., Bischoff A., and Stöffler D. 1992. Accretionary dust mantles in CM chondrites: Evidence for solar nebula processes. *Geochimica et Cosmochimica Acta* 56:2873–2897.

Metzler K., Bobe K.-D., Palme H., Spettel B., and Stöffler D. 1995. Thermal and impact metamorphism on the HED parent asteroid. *Planetary and Space Science* 43:499–525.

Mittlefehldt D. W., McCoy T. J., Goodrich C. A., and Kracher A. 1998. Non-chondritic meteorites from asteroidal bodies. In *Planetary materials*, vol. 36, edited by Papike J. J. Washington, D.C.: Mineralogical Society of America. pp. 4-1–4-195.

Mittlefehldt D. W., Herrin J. S., Quinn J. E., Mertzman S. A., Cartwright J. A., Mertzman K. R., and Peng Z. X. 2013. Composition and petrology of HED polymict breccias: The regolith of (4) Vesta. *Meteoritics & Planetary Science* 48:2105–2134.

Moriarty G. M., Rumble D. III, and Friedrich J. M. 2009. Compositions of four unusual CM or CM-related Antarctic chodrites. *Chemie der Erde* 69:161–168.

Nazarov M. A., Kurat G., Brandstaetter F., Ntaflos T., Chaussidon M., and Hoppe P. 2009. Phosphorous-bearing sulfides and their associations in CM Chondrites. *Petrology* 17:115–138.

Papike J. J. 1998. Comparative planetary mineralogy: Chemistry of melt-derived pyroxene, feldspar, and olivine. In *Planetary materials*, vol. 36. edited by Papike J. J. Washington, D.C.: Mineralogical Society of America. pp. 7-1–7-11.

Papike J. J., Karner J. M., and Shearer C. K. 2003. Determination of planetary basalt parentage: A simple technique using the electron microprobe. *American Mineralogist* 88:469–472.

Patzer A. and McSween H. Y. 2012. Ordinary (mesostasis) and not-so-ordinary (symplectites) late-stage assemblages in howardites. *Meteoritics & Planetary Science* 47:1475–1490.

Patzer A., Schlüter J., Schultz L., Hill D. H., and Boynton W. V. 2005. The new polymict eucrite Dar al Gani 983: Petrography, chemical composition, noble gas record, and evolution. *Meteoritics & Planetary Science* 40:869–879.

Poldervaart A. and Hess H. H. 1951. Pyroxenes in the crystallization of basaltic magma. *Journal of Geology* 59:472–489.

Pun A. and Papike J. J. 1995. Ion microprobe investigation of exsolved pyroxenes in cumulate eucrites: Determination of selected trace-element partition coefficients. *Geochimica et Cosmochimica Acta* 59:2279–2289.

Pun A. and Papike J. J. 1996. Unequilibrated eucrites and the equilibrated Juvinas eucrite: Pyroxene systematics and major, minor, and trace element zoning. *American Mineralogist* 81:1438–1451.

Pun A., Keil K., Taylor G. J., and Wieler R. 1998. The Kapoeta howardiate: Implications for the regolith evolution of the howardites-eucrite-diogenite parent body. *Meteoritics & Planetary Science* 33:835–851.

Rubin A. E., Trigo-Rodríguez J. M., Huber H., and Wasson J. T. 2007. Progressive aqueous alteration of CM carbonaceous chondrites. *Geochimica et Cosmochimica Acta* 71:2361–2382.

Rumble D. III and Hoering T. C. 1994. Analysis of oxygen and sulfur isotope ratios in oxide and sulfide minerals by spot heating with a carbon dioxide laser in a fluorine atmosphere. *Accounts of Chemical Research* 27:237–241.

Rumble D. III, Farquhar J., Young E. D., and Christensen C. P. 1997. In situ oxygen isotope analysis with an excimer laser using F2 and Br F5 reagents and O_2 gas as analyte. *Geochimica et Cosmochimica Acta* 61:4229–4234.

Rumble D. III, Miller M. F., Franchi I. A., and Greenwood R. C. 2007. Oxygen three-isotope fractionation lines in terrestrial silicate minerals: An inter-laboratory comparison of hydrothermal quartz and eclogitic garnet. *Geochimica et Cosmochimica Acta* 71:3592–3600.

Scott E. R. D., Greenwood R. C., Franchi I. A., and Saunders I. S. 2009. Oxygen isotopic constraints on the origin and parent bodies of the eucrites, diogenites, and howardites. *Geochimica et Cosmochimica Acta* 73:5835–5853.

Sharp Z. D. 1990. A laser-based microanalytical method for the in-situ determination of oxygen isotope ratios of silicates and oxides. *Geochimica et Cosmochimica Acta* 54:1353–1357.

Shearer C. K., Burger P., and Papike J. J. 2010. Petrogenetic relationships between diogenites and olivine diogenites: Implications for magmatism on the HED parent body. *Geochimica et Cosmochimica Acta* 74:4865–4880.

Takeda H. 1991. Comparisons of Antarctic and non-Antarctic achondrites and possible origin of the differences. *Geochimica et Cosmochimica Acta* 55:35–47.

Takeda H. 1997. Mineralogical records of early planetary processes on the howardite, eucrite, diogenite parent body with reference to Vesta. *Meteoritics & Planetary Science* 32:841–853.

Takeda H. and Graham A. L. 1991. Degree of equilibration of eucritic pyroxenes and thermal metamorphism of the earliest planetary crust. *Meteoritics* 26:129–134.

Treiman A. H. and Drake M. J. 1985. Basaltic volcanism on the eucrite parent body: Petrology and chemistry of the polymict eucrite ALHA80102. *Journal of Geophysical Research* 90:C619–C628.

Valley J. W., Kitchen N., Kohn M. J., Niendorf C. R., and Spicuzza M. J. 1995. UWG-2, a garnet standard for oxygen isotope ratios: Strategies for high precision and accuracy with laser heating. *Geochimica et Cosmochimica Acta* 59:5223–5231.

Warren P. H., Jerde E. A., Migdisova L. F., and Yaroshevsky A. A. 1990. Pomozdino: An anomalous, high MgO/FeO, yet REE-rich eucrite. *Proceedings, LPSC* 20:281–297.

Warren P. H., Kallemeyn G. W., Huber H., Ulff-Møller F., and Choe W. 2009. Siderophile and other geochemical constraints on mixing relationships among HED-meteoritic breccias. *Geochimica et Cosmochimica Acta* 73:5918–5943.

Wiechert U. H., Halliday A. N., Palme H., and Rumble D. III. 2004. Oxygen isotope evidence for rapid mixing of the HED meteorite parent body. *Earth and Planetary Science Letters* 221:373–382.

Wlotzka F. 1993. A weathering scale for the ordinary chondrites (abstract). *Meteoritics* 28:460.

Yamaguchi A., Taylor G. J., and Keil K. 1996. Global crystal metamorphism of the eucrite parent body. *Icarus* 124:97–112.

Yamaguchi A., Taylor G. J., Keil K., Floss C., Crozaz G., Nyquist L. E., Bogard D. D., Garrison D. H., Reese Y. D., Wiesmann H., and Shih C.-Y. 2001. Post-crystallization reheating and partial melting of eucrite EET 90020 by impact into the hot crust of 4 Vesta ~ 4.50 Ga ago. *Geochimica et Cosmochimica Acta* 65:3577–3599.

Yamaguchi A., Barrat J. A., Greenwood R. C., Shirari N., Okamoto C., Setoyanagi T., Ebihara M., Franchi I. A., and Bohn M. 2009. Crustal partial melting on Vesta: Evidence from highly metamorphosed eucrites. *Geochimica et Cosmochimica Acta* 73:7162–7182.

Zolensky M. E., Weisberg M. K., Buchanan P. C., and Mittlefehldt D. W. 1996. Mineralogy of carbonaceous chondrite clasts in HED achondrites and the Moon. *Meteoritics & Planetary Science* 31:518–537.

SUPPORTING INFORMATION

Additional supporting information may be found in the online version of this article:

Figure S1: Locations of samples obtained using a diamond-tipped drill to extract powered samples from 1 mm diameter holes for oxygen isotope analyses (Table 3). The slice was taken from one end of the NWA 5232 main mass.

Figure S2: Of the 42 clasts examined in detail, 23 belonged to the subophitic group (12 coarse-, 5 medium-, and 6 fine-grained), 7 to the granoblastic group (4 coarse-, 2 medium-, and 1 fine-grained), 2 to the breccia clast group, 1 to the cumulate eucrite clast group, 1 to the olivine-rich group, 1 to the pyroxene-lath group, 1 was an impact melt clast, and 6 were single-crystal clasts (4 of which compositionally fit with the coarse-grained subophitic groups).

Figure S3: Backscattered electron (BSE) image of medium-grained subophitic clast. The silicates in these clasts are pyroxene (Pyx) (with darker high-Ca exsolution lamellae), plagioclase (Pl), and silica (Si). White phases are opaques: chromite (Cr) ± ilmenite (Il) ± troilite (Tr).

Figure S4: A) Plagioclase compositional ranges for 11 individual eucritic clasts. Textures plotted here are cumulate (Cu), granoblastic (Gr), single crystal (SC), and subophitic (So). B) Clast plagioclase K (atoms per formula unit) versus an compositions plotted by texture.

Figure S5: Photograph of CM carbonaceous chondrite clast. Note the angularity of the clast and the localized fragmentation and mixing of CM fragments surrounding the clast.